

---

# Towards more holistic interpretability: A lightweight disentangled Concept Bottleneck Model

---

Gaoxiang Huang<sup>1</sup> Songning Lai<sup>1</sup> Yutao Yue<sup>1</sup>

## Abstract

Concept Bottleneck Models (CBMs) enhance interpretability by predicting human-understandable concepts as intermediate representations. However, existing CBMs often suffer from input-to-concept mapping bias and limited controllability, which restricts their practical utility and undermines the reliability of concept-based strategies. To address these challenges, we propose a Lightweight Disentangled Concept Bottleneck Model (LDCBM) that automatically groups visual features into semantically meaningful components without the need for region annotations. By introducing a filter grouping loss and joint concept supervision, our method improves the alignment between visual patterns and concepts, enabling more transparent and robust decision-making. Notably, experiments on three diverse datasets demonstrate that LDCBM achieves higher concept and class accuracy, outperforming previous CBMs in both interpretability and classification performance. Complexity analysis reveals that the parameter count and FLOPs of LDCBM are less than 5% higher than those of Vanilla CBM. Furthermore, background mask intervention experiments validate the model’s strong capability to suppress irrelevant image regions, further corroborating the high precision of the visual-concept mapping under LDCBM’s lightweight design paradigm. By grounding concepts in visual evidence, our method overcomes a fundamental limitation of prior models and enhances the reliability of interpretable AI.

---

<sup>1</sup>HKUST(GZ), Guangzhou, China. Correspondence to: Gaoxiang Huang <ghuang991@connect.hkust-gz.edu.cn>, Songning Lai <songninglai@hkust-gz.edu.cn>, Yutao Yue <yutaoyue@hkust-gz.edu.cn>.

## 1. Introduction

Deep learning has achieved unprecedented success in fields such as image recognition and natural language processing, driving the rapid development of AI and transforming daily life. However, its inherent “black-box” nature renders the decision-making process difficult to explain. In critical applications (e.g., healthcare, law, autonomous driving), high performance must be accompanied by interpretability and trustworthiness. To address the “black-box” problem, Explainable AI (XAI) has emerged (Rudin et al., 2021). It aims to reveal the internal mechanisms of models, enabling both experts and ordinary users to understand the rationale behind specific decisions. Among numerous XAI methods—such as Prototypical Networks (Snell et al., 2017) and Sparse Autoencoders (Thasarathan et al., 2025)—Concept Bottleneck Models (CBMs) (Koh et al., 2020) have attracted significant attention due to their unique “conceptualized” intermediate layers, spanning both computer vision and natural language processing (Yang et al., 2023) tasks. CBMs first identify human-understandable “concepts” (e.g., presence of a beard, wearing glasses) and subsequently make final predictions (e.g., identity verification) based on these concepts. This two-stage structure inherently provides interpretability, making CBMs well-suited for interpreting the relationship between an input image and its output class predictions via intermediate, human-understandable concepts.

Despite recent work narrowing the performance gap between CBMs and black-box models (Zarlenga et al., 2022; Xu et al., 2024; Kim et al., 2023; Shang et al., 2024; Lai et al., 2025), the interpretability of existing CBMs primarily stems from the transparency of the concept-to-label prediction. Fewer studies have addressed the opacity and lack of controllability in the input-to-concept mapping. As shown in Figure 1, concept predictions are frequently mislocalized. For instance, the most salient attributes of a bird (e.g., body, head, tail, bill) are often misidentified in the background or other irrelevant regions. Furthermore, attribute mapping can be biased across different regions; for example, a “throat” attribute may rely on visual patterns associated with the head and bill, despite the lack of visual connection. This leads to classifications based on spurious correlations (Srivastava et al.; Sheth & Kahou, 2023) and introduces data

bias (Luyten; Panousis et al.) that compromises subsequent interpretability strategies.

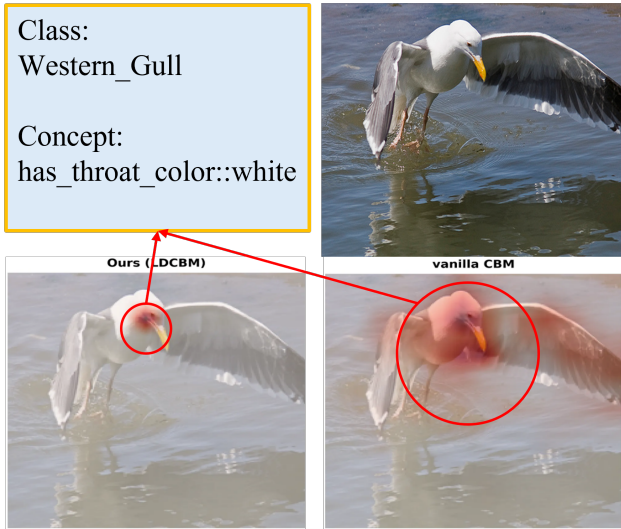


Figure 1. Case Study: Comparison between our proposed LDCBM and Vanilla CBM using inversion heatmap visualizations of visual pattern cluster relationships learned on the CUB dataset.

To bridge this gap, recent studies have attempted to improve input-to-concept interpretability through learnable prototypes and trustworthiness score alignment to approximate visual patterns and concepts (Huang et al., 2024; Zhang et al., 2025). However, these approaches often lack steerability, and prototypes are difficult to automatically align with concepts. Furthermore, DOT-CBMs (Xie et al., 2025) disentangle and extract priority image patches to align with concept ground truth. Yet, these crops depend excessively on regular patches and may fail to express the complete concept feature. Additionally, prototype-based methods (Tan et al., 2025) have been considered for alignment, but often merely calculate similarity without optimizing the target between prototypes and concepts. These methods either require significant manual effort to achieve disentanglement or rely on direct gradient-based methods that compromise the performance-interpretability trade-off.

In response to these limitations, we draw inspiration from the ICCNN (Shen et al., 2021; Mishra et al., 2024) and Prototypical Networks (Chen et al., 2025; Yu & Yang, 2025) frameworks, focusing on feature map-based analysis. We propose LDCBM to provide improved interpretability regarding the mutual visual region-concept relationship. Specifically, we introduce a lightweight, optimizable disentanglement of image components to automatically adjust the semantic composition, replacing rigid image grid cropping. This is achieved by using an auxiliary loss to group similar-sized feature maps in the backbone while separating distinct

groups. We supplement our approach with computational complexity analysis and intervention experiments to verify LDCBM’s lightweight nature and accurate mapping.

In summary, the key contributions of this work are as follows:

- We systematically analyze the key gap in visual-to-concept mapping and propose a method to improve it, which is applicable to various previous CBM architectures to enhance performance.
- We introduce LDCBM, which automatically disentangles the key components of the input by leveraging feature maps for more interpretable and precise concept prediction.
- Experimental results demonstrate that our model surpasses other improved CBMs and achieves higher performance on three datasets, covering a range from coarse to fine-grained and small to large scale.

## 2. Methodology

### 2.1. Preliminary

**Concept Bottleneck Models:** Black-box models with bottleneck on human-annotation concepts, which first predicts the concepts, then uses the predicted concepts to make a final prediction. A Concept Bottleneck Model (CBM) consists of two predictors: a *concept predictor* and a *class predictor*. Given a labeled dataset  $\mathcal{D} = \{(x^{(n)}, c^{(n)}, y^{(n)})\}_{n=1}^N$ , where the input  $x^{(n)} \in \mathcal{X}$ , the target  $y^{(n)} \in \mathcal{Y}$ , and the human-annotated concepts  $c^{(n)} \in \mathcal{C}$ , in this supervised concept-based model setting, the additional annotated concept vectors  $c^{(n)} \in \{0, 1\}^M$ ,  $M$  is the dimension of a concept. For a given input  $x$ , the concept predictor maps it to the concept space  $\mathcal{C}$ , denoted as  $g_{\mathcal{X} \rightarrow \mathcal{C}}$ . Then, the output of the first model, the concepts  $c$ , is taken as the sole input and mapped to the label  $y$ , denoted as  $f_{\mathcal{C} \rightarrow \mathcal{Y}}$ . Thus, the training process of CBMs is supervised to encourage the alignment of  $\hat{c} = g(x)$  and  $\hat{y} = f(g(x))$  with the true concept and class labels, respectively.

**Compositional Models:** To automatically learn compositional features (Sinha et al., 2024) without relying on human-annotated regions, we adopt the filter grouping mechanism from (Shen et al., 2021). Let  $\Omega$  be the set of all filters in a specific layer. We aim to partition  $\Omega$  into  $K$  disjoint groups  $A = \{A_1, A_2, \dots, A_K\}$ , such that  $\Omega = \bigcup_{k=1}^K A_k$  and  $A_i \cap A_j = \emptyset$  for  $i \neq j$ . The learning objective is to maximize the similarity within groups and minimize it between groups:

$$\mathcal{L}_g(\theta, A) = - \sum_{k=1}^K \frac{S_k^{\text{intra}}}{S_k^{\text{inter}}} = - \sum_{k=1}^K \frac{\sum_{u,v \in A_k} s_{uv}}{\sum_{u \in A_k, v \in \Omega} s_{uv}}, \quad (1)$$

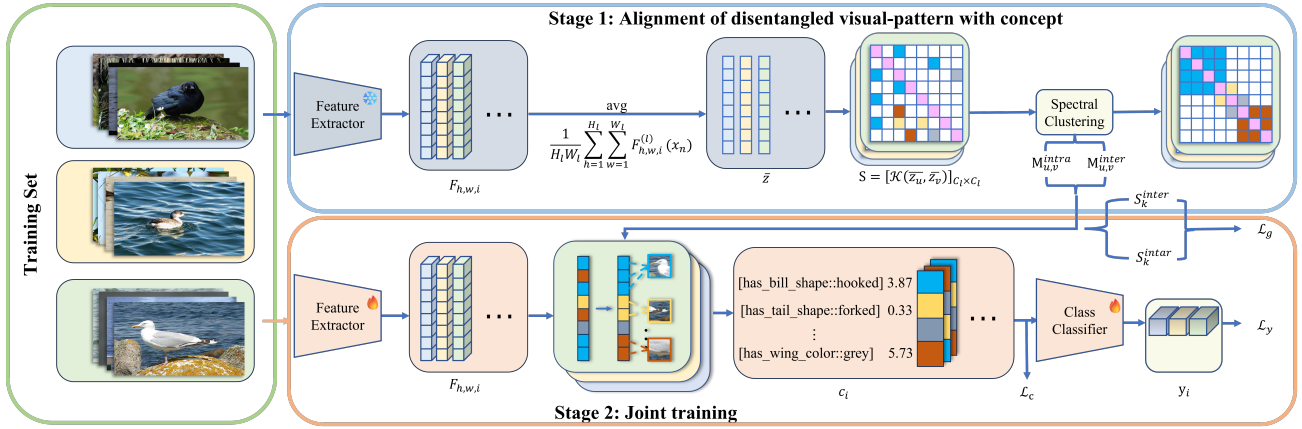


Figure 2. Overview of our LDCBM. It includes two stages modules: Alignment of disentangled visual-pattern with concept and Joint training among concept and class. The first forwards to get feature map and cluster for the intra and inter group mask what conduct the filter to concern specific visual pattern. The second do joint train from input to concept, and then mapping the concept to final task classification

where  $s_{uv}$  denotes the similarity between filter  $u$  and filter  $v$ . Here,  $S_k^{intra}$  aggregates the pairwise similarities of filters within group  $k$ , while  $S_k^{inter}$  sums the similarities between filters in group  $k$  and all other filters outside this group. By minimizing this ratio, filters within the same group are encouraged to learn coherent visual patterns, while different groups capture distinct, disentangled representations.

This method aim to improve the relationship in same group, that filters in a same group will learn the similar visual pattern. and minimize relationship between different groups, that filters in different groups are able to learn segmentable visual pattern.

## 2.2. Lightweight Disentangled Concept Bottleneck Models

As shown in Figure 2, our proposed LDCBM is conducted in two primary stages training: first, mapping the input image to a set of intermediate concepts, and second, mapping these concepts to the final class labels. The model is optimized by minimizing a total loss function,  $\mathcal{L}_{total}$ , defined as a weighted sum of three distinct components and is encouraged to minimize for LDCBM training:

$$\mathcal{L}_{total} = \mathcal{L}_y(f(c), y) + \lambda_c \mathcal{L}_c(g(x), c) + \lambda_g \mathcal{L}_g(\theta, A). \quad (2)$$

Here,  $\mathcal{L}_y$  represents the task loss for the final class prediction, which evaluates the output of the concept-to-label function  $f(c)$ .  $\mathcal{L}_c$  is the concept supervision loss for the middle concept prediction, applied to the output of the input-to-concept function  $g(x)$ . Finally,  $\mathcal{L}_g$  is a regularization term designed to encourage the disentanglement of learned features by structuring the parameters  $\theta$  of the feature extractor.

The hyperparameters  $\lambda_c$  and  $\lambda_g$  control the relative influence of the concept supervision and feature disentanglement objectives, respectively.

### 2.2.1. LEARNING DISENTANGLED VISUAL FEATURES

To achieve feature disentanglement, we first process an input image  $x_n$  through the initial layers of our network. Let  $F^{(l)}(x_n) \in \mathbb{R}^{H_l \times W_l \times C_l}$  denote the feature map produced by the  $l$ -th layer, where  $H_l$ ,  $W_l$ , and  $C_l$  are the height, width, and number of channels (Asbeh & Lerner, 2012), respectively. For each filter  $u \in \{1, \dots, C_l\}$ , we compute its global average response over the spatial dimensions ( $h, w$ ) for a given input  $x_n$ :

$$\bar{z}_u(x_n) = \frac{1}{H_l W_l} \sum_{h=1}^{H_l} \sum_{w=1}^{W_l} F_{h,w,u}^{(l)}(x_n), \quad (3)$$

This value,  $\bar{z}_u(x_n)$ , represents the overall activation of filter  $u$  for the image  $x_n$ . To measure the functional similarity between any two filters,  $u$  and  $v$ , we define a similarity metric,  $s_{uv}^{(l)}$ , based on the correlation of their global average responses across a batch of  $N$  images. This metric is implemented as a kernel function  $\mathcal{K}(\cdot, \cdot)$ :

$$\begin{aligned} s_{uv}^{(l)} &= \mathcal{K}(\bar{z}_u, \bar{z}_v) \\ &= \rho_{uv}^{(l)} + 1 \\ &= \frac{\frac{1}{N} \sum_{n=1}^N (\bar{z}_u(x_n) - \mu_u)(\bar{z}_v(x_n) - \mu_v)}{\sigma_u \sigma_v} + 1. \end{aligned} \quad (4)$$

Here,  $\rho_{uv}^{(l)} \in [-1, 1]$  is the Pearson correlation coefficient (Wang, 2013) between the activation vectors of filters  $u$

and  $v$  over the batch. We shift the coefficient by +1 to ensure the similarity score  $s_{uv}^{(l)}$  is non-negative, ranging from 0 (perfectly anti-correlated) to 2 (perfectly correlated). The terms  $\mu_u = \frac{1}{N} \sum_{n=1}^N \bar{z}_u(x_n)$  and  $\sigma_u^2 = \frac{1}{N} \sum_{n=1}^N (\bar{z}_u(x_n) - \mu_u)^2$  represent the mean and variance of the global average response for filter  $u$  across the batch.

After computing the similarity, the grouping threshold must be determined. This step follows (Shen et al., 2021), utilizing spectral clustering (Si & Zhu, 2013) to optimize the partition of the set of filters  $\Omega$  into groups  $A$ , as described in Equation 1. Based on these group assignments, we construct an intra-group mask  $M^{intra}$  and an inter-group mask  $M^{inter}$ . The masks are defined by the indicator function  $\mathbb{I}(\cdot)$ , such that  $M_{u,v}^{intra} = \mathbb{I}(z_u = z_v)$  for filters  $u, v$  in the same group, and  $M_{u,v}^{inter} = \mathbb{I}(z_u \neq z_v)$  for filters in different groups. Hence, we can easily calculate the inter and intra group similarity as follows:

$$\begin{aligned} -S_k^{intra} &= -\frac{1}{|M^{intra}|} \sum_{u,v} M_{u,v}^{intra} s_{uv}, \\ S_k^{inter} &= \frac{1}{|M^{inter}|} \sum_{u,v} M_{u,v}^{inter} s_{uv}. \end{aligned} \quad (5)$$

This allows us to formulate the disentanglement loss, which simultaneously maximizes the average similarity for filter pairs within the same group while minimizing the average similarity for pairs across different groups. This encourages filters within a group to learn functionally similar and cohesive representations.

Finally, this similarity matrix, containing all  $s_{uv}$  values with certain group separation, is then used to compute the disentanglement loss term,  $\mathcal{L}_g$ , as defined in Equation 1.

### 2.2.2. CONCEPT SUPERVISION

The disentanglement loss,  $\mathcal{L}_g$ , encourages filters to form semantically coherent groups by minimizing intra-group similarity and maximizing inter-group dissimilarity. This process establishes a latent association between visual patterns in the input image and specific filter groups. Building upon this structure, we introduce concept supervision to explicitly align these filter groups with human-understandable concepts.

Given a set of  $K$  filter groups, where each group  $A_k \in \mathcal{G}_i$ ,  $i \in \{1, \dots, M\}$  corresponds to a specific concept  $c_i$ , we aggregate the feature activations  $z_{\mathcal{G}_i}$  from the filters within that group. A concept classifier,  $g_c$ , which can be implemented as a simple linear layer, then maps these activations to a concept prediction. The concept supervision loss,  $\mathcal{L}_c$ , for a single concept is formulated using the Binary Cross-

Entropy (BCE) as follows:

$$\begin{aligned} \mathcal{L}_c &= \sum_i \text{BCE}(g_c(z_{\mathcal{G}_i}), c_i) \\ &= \sum_i \text{BCE}(w_i \cdot z_{\mathcal{G}_i} + b_i, c_i), \end{aligned} \quad (6)$$

where  $w_i$  and  $b_i$  are the learnable weights and bias for the  $i$ -th concept classifier. This loss ensures that the filters in group  $\mathcal{G}_i$ , already predisposed to activating on similar patterns due to  $\mathcal{L}_g$ , are jointly optimized to detect the presence of concept  $c_i$ . Consequently, the total objective for the first training stage, mapping inputs to concepts ( $X \rightarrow C$ ), is the combined minimization of  $\mathcal{L}_g$ .

### 2.2.3. CONCEPT-TO-CLASS PREDICTION

The second stage of our framework learns the mapping from the intermediate concept representations to the final class predictions. This is achieved by taking the vector of predicted concept activations,  $c = [c^{(1)}, c^{(2)}, \dots, c^{(N)}]$ , from the bottleneck layer and feeding it into a final linear classifier to produce the class logits,  $\hat{y}$ . Following the standard CBM architecture, this relationship is defined as:

$$\hat{y} = W_y \cdot c + b_y, \quad (7)$$

where  $W_y$  is the weight matrix and  $b_y$  is the bias vector of the final classification layer. The objective for this second stage ( $C \rightarrow Y$ ) is the standard cross-entropy(CE) classification loss,  $\mathcal{L}_y$ :

$$\mathcal{L}_y = \text{CE}(\hat{y}, y), \quad (8)$$

where  $y$  is the ground-truth class label. Finally, the entire model is trained end-to-end by optimizing the total loss,  $\mathcal{L}_{\text{total}}$ , as defined in Equation 2, which integrates the objectives from both training stages.

## 3. Experiments

**Datasets:** We evaluate different methods on three real-world datasets, which vary in granularity and scale.

- **Caltech-UCSD Birds-200-2011 (CUB)**(He & Peng, 2020) is a fine-grained dataset containing 11,788 images. It includes 312 human-annotated attributes. Following the data processing in (Koh et al., 2020), we use a subset of 112 attributes from 15 parts of the birds as our concepts.
- **Large-scale CelebFaces Attributes (CelebA)**(Liu et al., 2015) is a large-scale human-face dataset with over 200,000 images across 10,177 classes. Each image is annotated with 40 face attributes, which serve as our concepts.

- **Animals with Attributes 2 (AwA2)** (Xian et al., 2020) is a coarse-grained dataset containing 37,322 images and 50 animal classes. Each image is annotated with 85 attributes, which are used as concepts.

**Baselines.** We compare our proposed LDCBM with two established baselines: Vanilla CBM (Koh et al., 2020) and Concept Embedding Model (CEM) (Zarlenga et al., 2022). The concept labels and data-processing methods are adopted from the original CBM and ECBM (Xu et al., 2024) papers. For our proposed benchmark, we train the models for 200 epochs, with the exception of the LDCBM, which is trained for 400 epochs (performing a spectral cluster every 2 epochs) to ensure the same number of gradient updates. Then, aim to suit the dataset, we have access to the annotation strategies, choose the number of cluster 16, 32, 32 for datasets CUB, CelebA and Awa2 respectively.

### 3.1. Intervention Protocols

Concept interventions evaluate a model’s reliance on learned concepts by correcting erroneous predictions or corrupting correct ones, thereby quantifying interpretability. Our LDCBM supports test-time intervention. Unlike existing concept-based models that suffer from ambiguous inter-concept boundaries—leading to suboptimal concept and class classification—LDCBM disentangles object components to learn clear decision boundaries between concepts. This enhances feature utilization for each concept and improves overall performance.

A prevalent issue in CBMs is concept drift. Beyond measuring concept-class correlation, quantifying the association between image subjects and intermediate concepts is critical. Unlike other CBMs—whose insensitive response to interventions stems from misaligned visual-concept mappings caused by drift—LDCBM achieves more effective concept feature utilization and accurate visual pattern-concept-label alignment, resulting in stronger robustness to irrelevant disturbances.

**Concept Intervention** To evaluate the steerability of our model, we adopt the standard intervention protocol from CEM (Zarlenga et al., 2022). Specifically, we perform interventions at the concept embedding layer using RandInt regularization. During inference, the predicted concept probabilities are replaced with ground-truth labels at a controlled rate  $p_{\text{int}}$ . This allows us to strictly measure the model’s response to corrected conceptual information, verifying whether the decision-making process is truly guided by the learned concepts.

Notably, while vanilla CBM and CEM rely on these intervention schemes but suffer from insensitive responses due to poor visual-concept alignment, LDCBM’s disentangled fea-

ture representation ensures that the same interventions yield more interpretable changes in class predictions—directly validating its superior ability to model concept boundaries and resist drift.

**Background Mask** To assess whether LDCBM relies on spurious background correlations, we employ background replacement strategies on randomly sampled subsets of 200 CUB and 500 CelebA images for efficient evaluation. In the bird classification task, we utilize the **TravelingBirds** dataset (Koh et al., 2020), a CUB variant that retains identical semantic concepts but transplants foregrounds onto irrelevant background textures. Similarly, for the CelebA face attribute task, we simulate background shifts by suppressing environmental information via segmentation masks  $M$  derived from SAM (Kirillov et al., 2023). Specifically, we apply Gaussian blur  $\mathcal{G}_\sigma(\cdot)$  to the background regions:

$$\hat{x}_{h,w}^{\text{int}} = M_{h,w} \cdot x_{h,w} + (1 - M_{h,w}) \cdot \mathcal{G}_\sigma(x)_{h,w}. \quad (9)$$

Here,  $\mathcal{G}_\sigma(\cdot)$  represents a Gaussian blur operation with standard deviation  $\sigma \in [0, 5.0]$  controlling the blurring intensity. A value of  $\sigma = 0$  indicates no blurring (i.e., the original image), while increasing  $\sigma$  progressively suppresses the background information. By adjusting  $\sigma$ , we systematically investigate the model’s robustness under varying degrees of background interference.

### 3.2. Evaluation Protocols

**Standard Metrics** We use two metrics to evaluate the model’s performance: Concept Accuracy ( $C_{acc}$ ), which evaluates the model’s predictions for each concept individually, and Class Accuracy ( $A_{acc}$ ), which evaluates the overall classification task. The equations for these metrics are as follows:

$$C_{acc} = \frac{\sum_{n=1}^N \sum_{i=1}^M \mathbb{1}(c_i^{(n)} = \hat{c}_i^{(n)})}{N}, \quad (10)$$

$$A_{acc} = \frac{\sum_{n=1}^N \mathbb{1}(y^{(n)} = \hat{y}^{(n)})}{N}. \quad (11)$$

**Robustness Evaluation** Using the background masking protocol, we measure the stability of the model by calculating the relative performance drop. For a given metric  $\mathcal{A}$  (either  $A_{acc}$  or  $C_{acc}$ ), the drop is defined as:

$$\text{Drop} (\%) = \frac{\mathcal{A}_{\text{original}} - \mathcal{A}_{\text{masked}}}{\mathcal{A}_{\text{original}}} \times 100\%. \quad (12)$$

## 4. Result

### 4.1. LDCBM enhance the performance of both concept and class accuracy

Table 1 presents a comparative analysis of different models’ performance, specifically focusing on Concept and Class

Table 1. Generality Results in terms of Concept Accuracy and Class Accuracy. We evaluate models on CUB, CelebA, and AWA2 datasets. Bold indicates the best result, underline indicates the 2nd-best.

DATASET	MODEL	CONCEPT	CLASS
CUB	CBM	0.9220	0.6080
	CEM	<u>0.9350</u>	0.6572
	OURS	0.9291	<u>0.6617</u>
	CEM+OURS	<b>0.9386</b>	<b>0.6636</b>
CELEBA	CBM	0.9121	0.5115
	CEM	<u>0.9126</u>	0.5324
	OURS	0.9115	<u>0.5324</u>
	CEM+OURS	<b>0.9176</b>	<b>0.6350</b>
AWA2	CBM	0.9355	0.7663
	CEM	0.9366	0.7708
	OURS	<u>0.9400</u>	<u>0.7755</u>
	CEM+OURS	<b>0.9430</b>	<b>0.7841</b>

accuracy metrics across various datasets. All three evaluated models consistently achieve high concept accuracies, exceeding 90.0% with only marginal differences among them. However, LDCBM demonstrates a notable advantage in Class accuracy, particularly in challenging scenarios. On the large-scale CelebA dataset, LDCBM achieves the highest Class accuracy, matching CEM’s performance and surpassing CBM. Furthermore, in fine-grained tasks, such as those represented by the CUB dataset, LDCBM exhibits strong Class accuracy, closely approaching the top-performing CEM model and significantly outperforming CBM, while also maintaining a high concept accuracy. To further investigate the properties of LDCBM, we also evaluated the hybrid CEM+LDCBM model outperformed all three standalone models across all datasets. Notably, on the CelebA dataset, it achieved a class accuracy of 63.50%, surpassing CEM alone by approximately 10.26%. This substantial gain suggests that the disentanglement module from LDCBM enables the network to utilize concept information more effectively for classification.

This robust performance in Class accuracy, especially in fine-grained contexts, suggests that LDCBM effectively captures the pure and distinct features of concepts. These features are then robustly transferred to the interpretable decision-making process, ensuring that each concept functions as a unique and cognitively distinct component. This inherent capability not only enhances interpretability but also directly contributes to LDCBM’s superior Class accuracy compared to other methods.

This robust performance in Class accuracy, especially in fine-grained contexts, challenges the common trade-off between interpretability and performance. Intuitively, imposing disentanglement constraints might restrict model capacity. However, we provide a theoretical proof in Appendix A

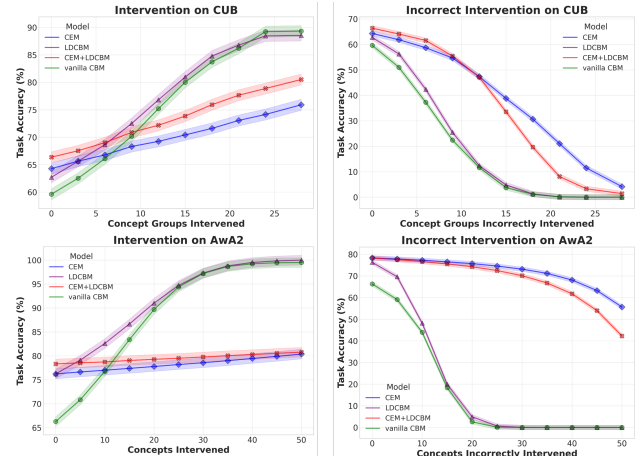


Figure 3. Intervention result of performing correct and incorrect randomly concept interventions in fine-grained and coarse-grained datasets (CUB and AWA2) respectively by four models. Following (Koh et al., 2020), intervention in CUB, we set groups of related concepts together.

demonstrating that our specific disentanglement loss reduces the generalization error bound, thereby explaining this counter-intuitive performance gain.

**Calculation Complexity Analysis** As demonstrated in Table 2, our LDCBM maintains a lightweight profile comparable to the Vanilla CBM while significantly outperforming it in interpretability. Specifically, LDCBM incurs negligible additional parameters and FLOPs compared to the backbone owing to its efficient disentanglement design. In terms of inference latency, LDCBM ( $\sim 6.18$ ms) is substantially faster than the high-performing CEM ( $\sim 10.09$ ms), making it a more practical choice for real-time applications where both transparency and speed are critical.

#### 4.2. LDCBM achieve the better efficiency trade-off Under Intervention

Concept interventions evaluate a model’s reliance on learned concepts by systematically correcting erroneous predictions or corrupting correct ones to observe the impact on final class accuracy. As depicted in Figure 3, we progressively intervene on four models—Vanilla CBM, CEM, LDCBM, and the hybrid CEM+LDCBM—using both fine-grained (CUB) and coarse-grained (AWA2) datasets.

Vanilla CBM exhibits highly sensitive accuracy curves, where task accuracy approaches 100% under full correct intervention and drops to nearly 0% under full corruption. However, its initial performance is relatively weak, starting at 60.80% on CUB. In contrast, CEM starts with significantly higher initial performance, achieving 66.36% on CUB and 77.08% on AWA2. Despite this strong baseline,

Table 2. Comparison of computational complexity. We report the quantity of parameters, FLOPs, and inference time per image for Vanilla CBM, CEM, and our proposed LDCBM. The spectral clustering time is listed separately as a training-only overhead.

MODEL	PARAMETERS (M)	FLOPS (G)	INFERENCE TIME (MS PER IMAGE)	DESCRIPTION
CBM	11.26	1.8236	~1.62	STANDARD RESNET18 + LINEAR HEAD
CEM	13.89	1.8262	~10.09	STANDARD RESNET18 + CEM LOGIC
LDCBM (OURS)	11.26	1.8236	~6.18	CUSTOM RESNET18 + LINEAR HEAD
<i>Spectral Clustering (Training-only Overhead)</i>				
128×128-SCALE: 178.0682 MS/SINGLE RUN				

CEM shows marginal improvement during correct intervention on Awa2, with final class accuracy reaching only 80.37%—a gain of just 4.1% even with 100% concept correction. Furthermore, under 100% corruption, the task accuracy on Awa2 decreases only moderately to 55.60%. These results highlight a clear trade-off: Vanilla CBM offers high interpretability but weak performance, whereas CEM offers strong performance but limited interpretability.

In comparison, our proposed LDCBM demonstrates a superior balance. On the CUB dataset, LDCBM improves initial task accuracy by 5.37% over Vanilla CBM while maintaining high sensitivity to concept interventions. Notably, the hybrid model CEM+LDCBM yields further benefits, boosting initial performance to 66.36%. Moreover, the sensitivity range of the accuracy curve expands by approximately 20% compared to CEM, making the model significantly more interpretable. These findings indicate that the disentanglement design of LDCBM effectively captures independent concept information and better aligns visual patterns with ground-truth concepts, resulting in a more interpretable and robust model.

### 4.3. LDCBM Establishes More Robust Visual-Concept Mapping

A fundamental challenge for CBMs lies in ensuring that their predictions are grounded in relevant visual features rather than spurious correlations such as background contextual information. To verify whether the LDCBM successfully anchors concepts to the inherent properties of objects themselves, the limitations of the model are evaluated through background mask intervention. Quantitative experimental results are reported in Table 3, where the relative performance drop after background removal is adopted as the primary metric to measure model robustness. Experimental results show that baseline models suffer severe performance degradation after mask processing, which indicates a strong reliance on environmental cues. In particular, the task accuracy of Vanilla CBM on the CUB dataset experiences a drastic drop of up to 59.46%. Similarly, despite the high initial performance of the CEM, its accuracy still decreases significantly by 43.31%, which reveals that its concept em-

beddings encode irrelevant background information to a certain extent. In contrast, models integrated with our LDCBM method exhibit superior robustness. The hybrid model (CEM+Ours) reduces the performance drop to 41.50% on the CUB dataset, and a more notable improvement is observed on the CelebA dataset, where the performance drop is reduced from 52.11% to 44.84%. This consistent ability to preserve task accuracy demonstrates that the LDCBM effectively steers the model to focus on foreground object regions instead of overfitting to background noise. Given that the relative drops in concept accuracy across all methods are at a comparable level, the stability of the LDCBM in the final classification stage provides compelling evidence that the concepts it learns possess higher visual fidelity to the objects themselves. By mitigating the Clever Hans effect, the LDCBM establishes a more reliable alignment between visual patterns and semantic concepts.

### 4.4. Qualitative Analysis: Feature Disentanglement Visualization

To intuitively verify the disentanglement capability of our method, we visualize the feature distributions before the concept layer using t-SNE. As illustrated in Figure 4, we compare the learned feature spaces of Vanilla CBM and LDCBM on the CUB dataset.

In Vanilla CBM, the feature points corresponding to different visual patterns are heavily entangled, suggesting that the model treats concepts as overlapping global features rather than distinct components. This entanglement explains its susceptibility to spurious correlations. In contrast, LDCBM effectively induces compact and well-separated feature clusters. Each cluster corresponds to a specific group of visual filters, demonstrating that our proposed grouping loss successfully forces the network to disentangle visual information into independent semantic units before mapping them to concepts. This clear structural separation validates LDCBM’s ability to learn more holistic and interpretable representations.

Table 3. Robustness evaluation against background shifts. We report Task and Concept Accuracy on CUB and CelebA datasets before and after background removal. The Drop (%) column indicates the relative performance degradation. Our models demonstrate significantly smaller performance drops compared to baselines, indicating that the learned concepts are firmly grounded in foreground objects rather than spurious background correlations.

DATASET	MODEL (VARIANT)	TASK ACCURACY			CONCEPT ACCURACY		
		ORIGINAL (↑)	MASKED (↓)	DROP (%) (↓)	ORIGINAL (↑)	MASKED (↓)	DROP (%) (↓)
CUB	CBM	0.5550	0.2250	59.46	0.9266	0.8821	4.80
	CBM + OURS	0.5800	0.3150	45.69	0.9381	0.8869	5.46
	CEM	0.6880	0.3900	43.31	0.9366	0.8814	5.89
	CEM + OURS	0.6940	0.4060	41.50	0.9414	0.8758	6.96
CELEBA	CBM	0.2400	0.1440	40.00	0.9076	0.8774	3.33
	CBM + OURS	0.2520	0.1800	28.57	0.9137	0.8791	3.79
	CEM	0.2840	0.1360	52.11	0.8899	0.8625	3.08
	CEM + OURS	0.4460	0.2460	44.84	0.8937	0.8697	2.69

↑: HIGHER VALUE IS BETTER; ↓: LOWER IS BETTER; -: RESULTS NOT COMPLETED.

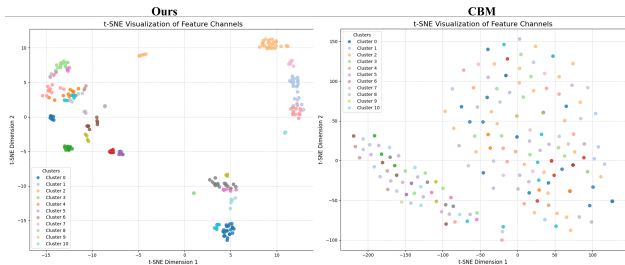


Figure 4. t-SNE visualization of learned visual features on the CUB dataset. While Vanilla CBM shows entangled feature distributions (left), LDCBM (right) forms distinct, semantically meaningful clusters, indicating effective disentanglement of visual patterns.

## 5. Conclusion and limitation

This paper aims to address the limitations of CBMs regarding input-to-concept mapping bias and to simplify the complexity associated with prior methods. We propose LDCBM, a lightweight and automated method to recognize meaningful visual patterns without requiring region annotations or image patching. Specifically, our method automatically identifies optimal alignments between concept ground truth and visual features. By introducing a filter grouping loss to separate distinct semantic areas and utilizing joint concept supervision, we achieve accurate alignment between semantic regions and concept ground truth. Experiments demonstrate the effectiveness of our method. The supplementary computational complexity analysis and background masking experiments provide direct evidence that the proposed lightweight design effectively breaks the performance-interpretability trade-off. Specifically, these results validate the method from the dual perspectives of engineering feasibility and the faithfulness of semantic mapping. LDCBM not only makes the input-to-concept mapping more transparent and responsible but also provides an in-depth analysis

of the interpretability-performance trade-off, contributing to the reduction of potential risks in CBMs and moving towards a more reliable future for AI.

## 6. Impact Statement

This paper presents work whose goal is to advance the field of machine learning. There are many potential societal consequences of our work, none of which we feel must be specifically highlighted here.

## References

- Asbeh, N. and Lerner, B. Learning Latent Variable Models by Pairwise Cluster Comparison. In *Proceedings of the Asian Conference on Machine Learning*, pp. 33–48. PMLR, November 2012.
- Chen, R., Xia, H., Xia, S., Shao, M., and Ding, Z. IP-Net: Interpretable Prototype Network for Multi-Source Domain Adaptation. In *ICASSP 2025 - 2025 IEEE International Conference on Acoustics, Speech and Signal Processing (ICASSP)*, pp. 1–5, April 2025. doi: 10.1109/ICASSP49660.2025.10888604.
- He, X. and Peng, Y. Fine-grained Visual-textual Representation Learning. *IEEE Transactions on Circuits and Systems for Video Technology*, 30(2):520–531, February 2020. ISSN 1051-8215, 1558-2205. doi: 10.1109/TCSVT.2019.2892802.
- Huang, Q., Song, J., Hu, J., Zhang, H., Wang, Y., and Song, M. On the Concept Trustworthiness in Concept Bottleneck Models, March 2024.
- Kim, E., Jung, D., Park, S., Kim, S., and Yoon, S. Probabilistic Concept Bottleneck Models, June 2023.

- Kirillov, A., Mintun, E., Ravi, N., Mao, H., Rolland, C., Gustafson, L., Xiao, T., Whitehead, S., Berg, A. C., Lo, W.-Y., Dollár, P., and Girshick, R. Segment anything. *arXiv:2304.02643*, 2023.
- Koh, P. W., Nguyen, T., Tang, Y. S., Mussmann, S., Pierson, E., Kim, B., and Liang, P. Concept Bottleneck Models, December 2020.
- Lai, S., Liao, M., Hu, Z., Yang, J., Chen, W., Xiao, H., Tang, J., Liao, H., and Yue\*, Y. Learning New Concepts, Remembering the Old: Continual Learning for Multimodal Concept Bottleneck Models. In *Proceedings of the ACM International Conference on Multimedia (ACM MM 2025, BNI Oral, top-tier conference in artificial intelligence, BNI = outstanding papers in the main conference, h5-index 119)*, 2025.
- Liu, Z., Luo, P., Wang, X., and Tang, X. Deep Learning Face Attributes in the Wild, September 2015.
- Luyten, M. R. A Theoretical design of Concept Sets: Improving the predictability of concept bottleneck models.
- Mishra, S., Zhu, P., and Saligrama, V. Interpretable Compositional Representations for Robust Few-Shot Generalization. *IEEE Transactions on Pattern Analysis and Machine Intelligence*, 46(3):1496–1512, March 2024. ISSN 1939-3539. doi: 10.1109/TPAMI.2022.3212633.
- Panousis, K. P., Ienco, D., and Marcos, D. Coarse-to-Fine Concept Bottleneck Models.
- Rudin, C., Chen, C., Chen, Z., Huang, H., Semenova, L., and Zhong, C. Interpretable Machine Learning: Fundamental Principles and 10 Grand Challenges, July 2021.
- Shang, C., Zhou, S., Zhang, H., Ni, X., Yang, Y., and Wang, Y. Incremental Residual Concept Bottleneck Models. In *Proceedings of the IEEE/CVF Conference on Computer Vision and Pattern Recognition*, pp. 11030–11040, 2024.
- Shen, W., Wei, Z., Huang, S., Zhang, B., Fan, J., Zhao, P., and Zhang, Q. Interpretable Compositional Convolutional Neural Networks, July 2021.
- Sheth, I. and Kahou, S. E. Auxiliary Losses for Learning Generalizable Concept-based Models, November 2023.
- Si, Z. and Zhu, S.-C. Learning AND-OR Templates for Object Recognition and Detection. *IEEE Transactions on Pattern Analysis and Machine Intelligence*, 35(9):2189–2205, September 2013. ISSN 1939-3539. doi: 10.1109/TPAMI.2013.35.
- Sinha, S., Prensri, T., and Kordjamshidi, P. A Survey on Compositional Learning of AI Models: Theoretical and Experimental Practices, November 2024.
- Snell, J., Swersky, K., and Zemel, R. S. Prototypical Networks for Few-shot Learning, June 2017.
- Srivastava, D., Yan, G., and Weng, T.-W. VLG-CBM: Training Concept Bottleneck Models with Vision-Language Guidance.
- Tan, A., Zhou, F., and Chen, H. Explain via Any Concept: Concept Bottleneck Model with Open Vocabulary Concepts. In Leonardis, A., Ricci, E., Roth, S., Rusakovsky, O., Sattler, T., and Varol, G. (eds.), *Computer Vision – ECCV 2024*, pp. 123–138, Cham, 2025. Springer Nature Switzerland. ISBN 978-3-031-73016-0. doi: 10.1007/978-3-031-73016-0\_8.
- Thasarathan, H., Forsyth, J., Fel, T., Kowal, M., and Derpanis, K. Universal Sparse Autoencoders: Interpretable Cross-Model Concept Alignment, February 2025.
- Wang, J. Pearson Correlation Coefficient. In *Encyclopedia of Systems Biology*, pp. 1671–1671. Springer, New York, NY, 2013. ISBN 978-1-4419-9863-7. doi: 10.1007/978-1-4419-9863-7\_372.
- Xian, Y., Lampert, C. H., Schiele, B., and Akata, Z. Zero-Shot Learning – A Comprehensive Evaluation of the Good, the Bad and the Ugly, September 2020.
- Xie, Y., Zeng, Z., Zhang, H., Ding, Y., Wang, Y., Wang, Z., Chen, B., and Liu, H. Discovering Fine-Grained Visual-Concept Relations by Disentangled Optimal Transport Concept Bottleneck Models, May 2025.
- Xu, X., Qin, Y., Mi, L., Wang, H., and Li, X. Energy-Based Concept Bottleneck Models: Unifying Prediction, Concept Intervention, and Probabilistic Interpretations, December 2024.
- Yang, Y., Panagopoulou, A., Zhou, S., Jin, D., Callison-Burch, C., and Yatskar, M. Language in a Bottle: Language Model Guided Concept Bottlenecks for Interpretable Image Classification, April 2023.
- Yu, A. and Yang, Y.-B. Prototypical Part Transformer for Interpretable Image Recognition. In *ICASSP 2025 - 2025 IEEE International Conference on Acoustics, Speech and Signal Processing (ICASSP)*, pp. 1–5, April 2025. doi: 10.1109/ICASSP49660.2025.10890753.
- Zarlenga, M. E., Barbiero, P., Ciravegna, G., Marra, G., Giannini, F., Diligenti, M., Shams, Z., Precioso, F., Melacci, S., Weller, A., Lio, P., and Jamnik, M. Concept Embedding Models: Beyond the Accuracy-Explainability Trade-Off, December 2022.
- Zhang, R., Du, X., Yan, J., and Zhang, S. The Decoupling Concept Bottleneck Model. *IEEE Transactions on Pattern Analysis and Machine Intelligence*, 47(2):

1250–1265, February 2025. ISSN 1939-3539. doi:  
10.1109/TPAMI.2024.3489597.

## A. Theoretical Proofs for Lightweight Disentangled Concept Bottleneck Model (LDCBM)

### A.1. Preliminary Lemma 1 (Information Bottleneck Generalization Bound)

For any deep learning model, its generalization error  $\epsilon_{\text{gen}}$  satisfies the following upper bound:

$$\epsilon_{\text{gen}} \lesssim \sqrt{\frac{2^{I(X;T)}}{N}}$$

where  $T$  denotes the intermediate representation of the model,  $I(X;T)$  is the mutual information between the input and the intermediate representation, and  $N$  is the number of training samples. This lemma indicates that the smaller the mutual information between the intermediate representation and the input, the tighter the upper bound of the generalization error.

### A.2. Preliminary Lemma 2 (Basic Properties of Mutual Information)

1. Non-negativity:  $I(A; B) \geq 0$ , with equality if and only if  $A$  and  $B$  are mutually independent;
2. Chain rule:  $I(X; (Z_1, Z_2)) = I(X; Z_1) + I(X; Z_2 | Z_1)$ ;
3. Decomposition of conditional mutual information:  $I(Y; X | \hat{C}) = I(Y; Z_{\text{residual}} | \hat{C}) + I(Y; Z_{\text{concept}} | \hat{C}, Z_{\text{residual}})$ .

### A.3. Formal Definition of Concept Leakage

Concept leakage is a core flaw of Concept Bottleneck Models (CBMs). Its essence lies in the bottleneck layer failing to capture all information required for predicting  $Y$ , leading residual information (mostly spurious correlations) to still participate in the prediction process. A rigorous definition based on mutual information is given as follows:

**Definition 1 (Concept Leakage)** Given the predicted concepts  $\hat{C}$  of LDCBM, the model is said to suffer from concept leakage if the following condition holds:

$$\text{Leakage}(\hat{C}) = I(Y; X | \hat{C}) > 0$$

where  $I(Y; X | \hat{C})$  denotes the conditional mutual information, representing that the input  $X$  still contains valid information about the target  $Y$  given  $\hat{C}$  (i.e.,  $\hat{C}$  is not a sufficient statistic of  $Y$ ).

### A.4. Optimization Objective and Disentanglement Loss of LDCBM

LDCBM introduces a disentanglement loss on top of the standard CBM, with its core optimization objective defined as:

$$\mathcal{L}_{\text{LDCBM}} = \mathcal{L}_{\text{task}}(f(\hat{C}), Y) + \lambda_1 \mathcal{L}_{\text{concept}}(\hat{C}, C_{\text{gt}}) + \lambda_2 \mathcal{L}_{\text{dis}}$$

where:

- $\mathcal{L}_{\text{task}}$  is the task loss (e.g., cross-entropy);
- $\mathcal{L}_{\text{concept}}$  is the concept supervision loss (aligning predicted concepts with ground-truth concepts  $C_{\text{gt}}$ );
- $\lambda_1, \lambda_2$  are regularization coefficients;
- The disentanglement loss  $\mathcal{L}_{\text{dis}}$  is defined as:

$$\mathcal{L}_{\text{dis}} = I(Z_{\text{concept}}; Z_{\text{residual}})$$

The optimization goal is to minimize  $\mathcal{L}_{\text{dis}}$ , which enforces mutual independence between the concept subspace  $Z_{\text{concept}}$  and the residual subspace  $Z_{\text{residual}}$ .

### A.5. Proposition 1: Suppression of Concept Leakage by LDCBM

**Proposition 1** If the disentanglement loss of LDCBM converges to  $\mathcal{L}_{\text{dis}} \rightarrow 0$ , then its concept leakage satisfies:

$$\text{Leakage}(\hat{C}) \leq I(Y; Z_{\text{residual}})$$

Furthermore, when  $Z_{\text{residual}}$  is independent of  $Y$ ,  $\text{Leakage}(\hat{C}) \rightarrow 0$  (no concept leakage).

**Proof 1** First, decompose the input  $X$  into the joint representation of the concept subspace and the residual subspace:  $X \triangleq (Z_{\text{concept}}, Z_{\text{residual}})$ . By the chain rule of mutual information:

$$I(Y; X | \hat{C}) = I(Y; Z_{\text{concept}}, Z_{\text{residual}} | \hat{C}) = I(Y; Z_{\text{concept}} | \hat{C}) + I(Y; Z_{\text{residual}} | \hat{C}, Z_{\text{concept}})$$

In LDCBM,  $\hat{C}$  is the supervised output of  $Z_{\text{concept}}$  ( $\hat{C} = g(Z_{\text{concept}})$ , where  $g$  is a deterministic mapping). Thus, all information of  $Z_{\text{concept}}$  is fully contained in  $\hat{C}$ , implying  $I(Y; Z_{\text{concept}} | \hat{C}) = 0$ . Substituting this into the above equation yields:

$$I(Y; X | \hat{C}) = I(Y; Z_{\text{residual}} | \hat{C}, Z_{\text{concept}})$$

By the monotonic non-increase property of conditional mutual information ( $I(A; B|C) \leq I(A; B)$ ), we have:

$$I(Y; Z_{\text{residual}} | \hat{C}, Z_{\text{concept}}) \leq I(Y; Z_{\text{residual}})$$

Combining with Definition 1, we obtain:

$$\text{Leakage}(\hat{C}) = I(Y; X | \hat{C}) \leq I(Y; Z_{\text{residual}})$$

When  $\mathcal{L}_{\text{dis}} = I(Z_{\text{concept}}; Z_{\text{residual}}) \rightarrow 0$ ,  $Z_{\text{concept}}$  and  $Z_{\text{residual}}$  are mutually independent. The concept supervision loss  $\mathcal{L}_{\text{concept}}$  of LDCBM enforces  $Z_{\text{concept}}$  to encode only causal features  $Z_{\text{inv}}$  (strongly correlated with  $Y$ ), so  $Z_{\text{residual}}$  contains only spurious features  $Z_{\text{spu}}$ . If  $Z_{\text{spu}}$  is independent of  $Y$  during training (via invariance constraints), then  $I(Y; Z_{\text{residual}}) \rightarrow 0$ , and consequently  $\text{Leakage}(\hat{C}) \rightarrow 0$ .

### A.6. Proposition 2: Generalization Error Bound of LDCBM

**Proposition 2** Let the intermediate representation of a standard black-box model (e.g., ResNet) be  $Z_{\text{BB}}$  (dimension  $d$ ), the intermediate representation of a standard CBM be  $C$  (dimension  $k$ ), and the intermediate representation of LDCBM be  $\hat{C}$  (dimension  $k$ ), with  $k \ll d$ . Then the upper bounds of their generalization errors satisfy:

$$\epsilon_{\text{gen}}^{\text{LDCBM}} < \epsilon_{\text{gen}}^{\text{Standard CBM}} < \epsilon_{\text{gen}}^{\text{Black-box}}$$

**Proof 2** For black-box models: Black-box models have no structural constraints. To minimize the task loss, they maximize  $I(X; Z_{\text{BB}})$  to retain all input information (including noise and spurious correlations), so  $I(X; Z_{\text{BB}}) \approx H(X)$  (the entropy of the input). By Preliminary Lemma 1, its generalization error bound is:

$$\epsilon_{\text{gen}}^{\text{Black-box}} \lesssim \sqrt{\frac{2H(X)}{N}}$$

For standard CBMs: Standard CBMs restrict the dimension of the intermediate representation to  $k$  via concept supervision, so  $I(X; C) \leq H(C) \ll H(X)$  (since  $C$  consists of low-dimensional semantic concepts). Its generalization error bound is:

$$\epsilon_{\text{gen}}^{\text{Standard CBM}} \lesssim \sqrt{\frac{2H(C)}{N}}$$

Since  $H(C) \ll H(X)$ , it follows that  $\epsilon_{\text{gen}}^{\text{Standard CBM}} < \epsilon_{\text{gen}}^{\text{Black-box}}$ .

For LDCBM: LDCBM introduces the disentanglement loss  $\mathcal{L}_{\text{dis}} = I(Z_{\text{concept}}; Z_{\text{residual}}) \rightarrow 0$  on top of standard CBM, meaning  $Z_{\text{concept}}$  and  $Z_{\text{residual}}$  are independent. In this case:

$$I(X; \hat{C}) = I((Z_{\text{concept}}, Z_{\text{residual}}); \hat{C}) = I(Z_{\text{concept}}; \hat{C}) + I(Z_{\text{residual}}; \hat{C} | Z_{\text{concept}})$$

Since  $\hat{C}$  is generated solely by  $Z_{\text{concept}}$ ,  $I(Z_{\text{residual}}; \hat{C} | Z_{\text{concept}}) = 0$ , so  $I(X; \hat{C}) = I(Z_{\text{concept}}; \hat{C})$ .

Furthermore, the disentanglement loss enforces  $Z_{\text{concept}}$  to encode only minimal sufficient causal features, so  $I(Z_{\text{concept}}; \hat{C}) < H(C)$  (the  $I(X; C)$  of standard CBM contains partial spurious information). Substituting into Preliminary Lemma 1 gives:

$$\epsilon_{\text{gen}}^{\text{LDCBM}} \lesssim \sqrt{\frac{2I(Z_{\text{concept}}; \hat{C})}{N}} < \sqrt{\frac{2H(C)}{N}} = \epsilon_{\text{gen}}^{\text{Standard CBM}}$$

In summary, the upper bounds of the generalization errors for the three models satisfy  $\epsilon_{\text{gen}}^{\text{LDCBM}} < \epsilon_{\text{gen}}^{\text{Standard CBM}} < \epsilon_{\text{gen}}^{\text{Black-box}}$ .